Advances in Geo-Energy Research

Vol. 2, No. 1, p. 43-52, 2018
www.astp-agr.com

Original article

Experimental study on evolution behaviors of triaxial-shearing parameters for hydrate-bearing intermediate fine sediment

Yanlong Li[1,2], Changling Liu[1,2*], Lele Liu[1,2], Jianye Sun[1,2], Haojia Liu[1,3], Qingguo Meng[1,2]

[1]*Key Laboratory of Gas Hydrate, Ministry of Land and Resource, Qingdao Institute of Marine Geology, Qingdao 266071, P. R. China*

[2]*Laboratory for Marine Mineral Resource, Qingdao National Laboratory for Marine Science, Qingdao 266071, P. R. China*

[3]*School of Petroleum Engineering, China Univercity of Petroleum, Qingdao 266580, P. R. China*

(Received January 3, 2018; revised January 27, 2018; accepted January 28, 2018; available online February 2, 2018)

Citation:
Li, Y., Liu, C., Liu, L., Sun, J., Liu, H., Meng, Q. Experimental study on evolution behaviors of triaxial-shearing parameters for hydrate-bearing intermediate fine sediment. *Advances in Geo-Energy Research*, 2018, 2(1): 43-52, doi: 10.26804/ager.2018.01.04.

Corresponding author:
*E-mail: qdliuchangling@163.com

Keywords:
Hydrate-bearing sediments
strain-hardening
strain-softening
triaxial shear strength
intermediate fine sediment

Abstract:
Evolution behaviors of triaxial shearing parameters are very important for geo-technical response analysis during the process of extracting natural gas from hydrate-bearing reservoirs. In order to explore the effects of hydrate formation/decomposition on triaxial shearing behaviors of intermediate fine sediment, natural beach sand in Qingdao, China, which was sieved from 0.1 mm to 0.85 mm, was used and a series of triaxial shear tests were carried out in this paper. The principle of critical state was firstly used to explain the mechanism of strain softening and/or hardening failure mode. Moreover, an empirical model was provided for axial-lateral strain and corresponding model parameters calculation. Evolution rules of critical strength parameters were analyzed prominently. The results show that failure mode of sediment is controlled by several parameters, such as effective confining pressure, hydrate saturation, etc. Different axial-lateral strain model coefficients' effect on strain relationships are different, probing into the physical meaning of each coefficient is essential for further understanding of strain relationships. Complex geo-technical response should be faced with the progress of producing natural gas from hydrate-bearing reservoir, because of sudden change of failure pattern and formation modulus. Further compressive study on critical condition of failure pattern is needed for proposed promising hydrate-bearing reservoirs.

1. Introduction

Gas hydrate is a caged compound formed under high pressure and low temperature conditions, it was anticipated to be a promising energy resource (Zhang et al., 2007; Wu et al., 2017). Hydrate-bearing reservoir is always formed by unconsolidated formation. Thus, production of natural gas from hydrate-bearing reservoir may lead complex geo-mechanical response, which will affect the stability of wellbore or other subsea structures (Winters et al., 2014). Therefore, prediction of geo-mechanical properties of hydrate-bearing sediments is essential to avoid the occurrence of geo-hazards and ensure gas productivity (Wei et al., 2011; Li et al., 2012; Liu et al., 2013).

Triaxial shearing test is one of the direct and effective ways to obtain mechanical properties of hydrate-bearing sediments. Because of lack of pressure coring samples, artificial reconstructed hydrate-bearing samples are widely used for detection of triaxial shearing test. Previous studies have published lots of experimental research results on triaxial shearing test of hydrate-bearing sediments, and these researches already made tremendous progress in hydrate-bearing sample preparation methods (Yun et al., 2007; Masui et al., 2007, 2015; Priest et al., 2014), hydrate saturation decision methods (Liu et al., 2014; Li et al., 2016), shearing rate control (Yu et al., 2011; Li et al., 2011, 2012) and shearing P-T condition selection(Yan et al., 2012, 2013; Li et al., 2017). Both artificial (Winters et al., 2007; Miyazaki et al., 2011) and field coring samples (Hyodo et al., 2013; Winters et al., 2014; Shi et al., 2014, 2015) were used for triaxial shearing test. Different research results already showed various shearing behaviors for hydrate-bearing sediments, which can be divided into strain-hardening failure mode and/or strain-softening failure mode totally (Lu et al., 2007; Zhang et al., 2010, 2011; Sun et al., 2012). However, the above researches rarely consider the strain softening and/or strain-hardening mechanisms, axial strain vs lateral/volumetric strain relationships, as well as their critical changing conditions under triaxial shearing condition. Miyazaki et al. (2012) provided a preliminary model for axial strain vs lateral strain

https://doi.org/10.26804/ager.2018.01.04.

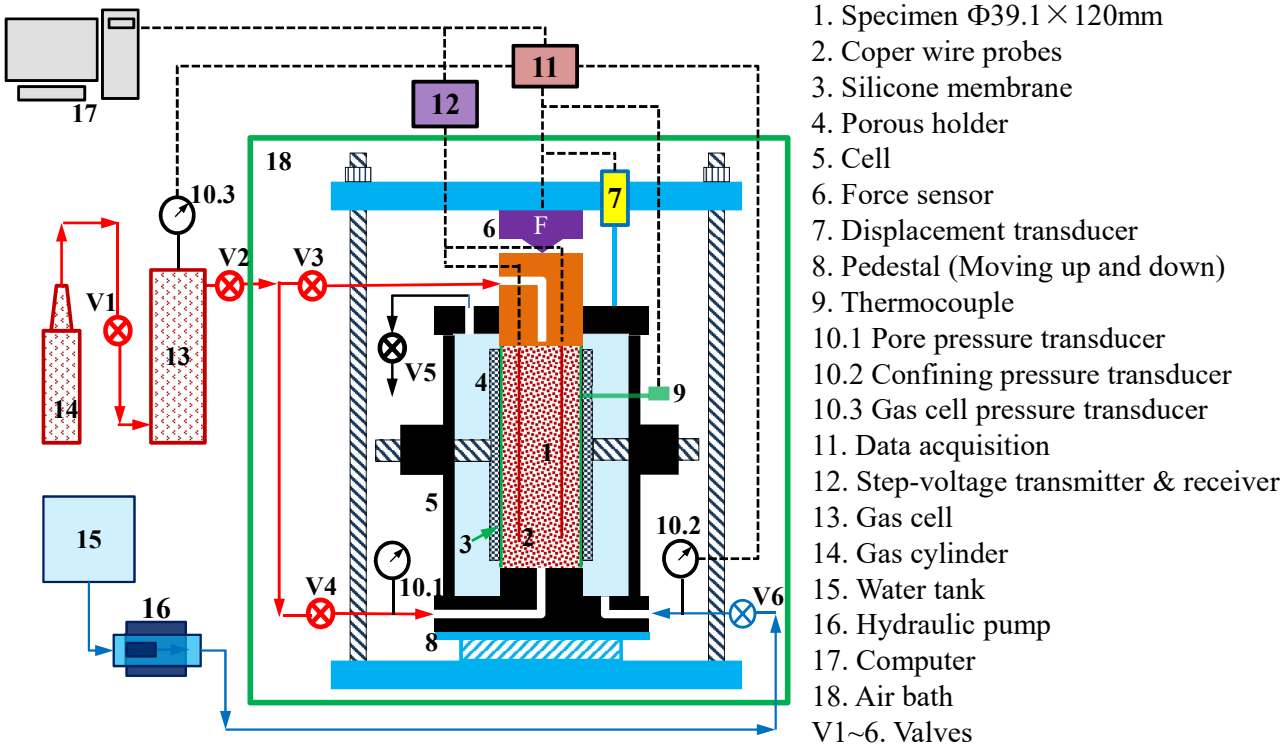

Fig. 1. Schematic of triaxial apparatus for hydrate-bearing sediments.

relationship by ignoring the influences of hydrate saturation. What's more, this model can't describe axial-volumetric strain changing rules of hydrate-bearing sediments under triaxial shearing conditions.

In this paper, a series of triaxial shear test were carried out to explore deformation and failure behaviors of unconsolidated sediments with different saturation of methane hydrate. The principle of critical state was firstly used to explain the mechanism of strain softening and hardening failure mode. Secondly, axial-lateral strain relationships were explored, and then a semi-empirical model was provided for axial-lateral strain relationships description. Finally, evolution behaviors of typical triaxial shearing parameters along with hydrate saturation and effective confining pressure were analyzed based on failure mode. This study may have some significant guide for the modeling of mechanical parameters of hydrate-bearing sediments.

2. Measurement method and experimental process

2.1 Test apparatus and sample preparation

The triaxial system for testing hydrate-bearing sediments is illustrated in Fig. 1. It was a modified soil triaxial apparatus with additional features, such as pressure controller and air bath cooler, was developed to reproduce the high-pressure, low-temperature conditions of deep seabed sediments for hydrate formation and subsequent triaxial shearing tests. The apparatus is equipped with a hydraulic system that can provide and maintain confining pressure up to 10 MPa. By lowering the air temperature surrounding the triaxial cell within the air bath, water and percolating gas inside the triaxial specimen were cooled, sufficient time should be allowed for the system to reach hydrate equilibrium. A thermocouple (No. 9 in Fig. 1) placed inside the cell near the middle of the specimen records specimen temperature evolution over time. In these experiments, the temperature was always kept above freezing. Controls for the confining pressure and temperature systems were established using data control and acquisition software. Appropriate calibrations were made for changes in pressure and temperature and trace changes in TDR.

Methane gas with purity of 99.99% was used in the experiment.

To avoid the influence of shale content and other minerals, marine silica intermediate fine sands with dry density of 2.78 g/cm^3 were used for formation of hydrate-bearing samples. Sample size is Φ39.1 mm × 120 mm. Particle size analysis curve of intermediate fine sands is illustrated in Fig. 2.

Solution with SDS mass concentration of 0.03% was used to promote the formation of methane hydrate in porous media and detailed sample preparation procedure are as follows. ① 192 g dry sands were intensively mixed with 8 mL, 16 mL and 24 mL SDS solution, respectively. After 24 hours' standing in an enclosed container, go through next step. It should be note that for triaxial shearing test of sediments without hydrate, the above process can be omitted. ② Mixed sediments were put into the silicone membrane which stands within the high pressure reactor with four times (about 48 g each time for dry sands). Meanwhile, apply moderate compaction. Thickness of

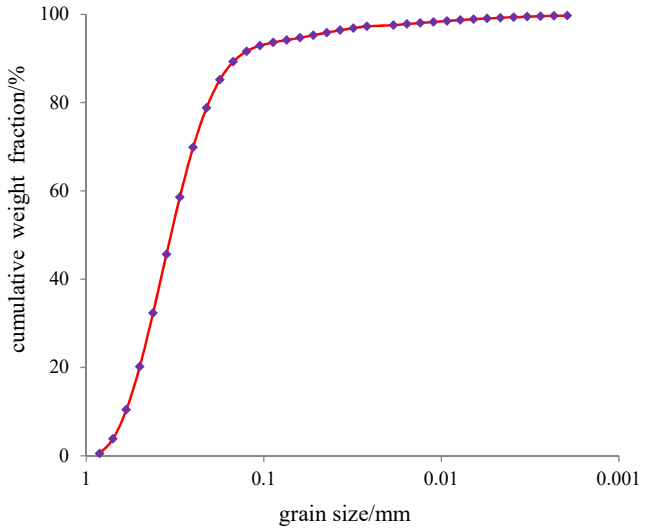

Fig. 2. Sand particle size distribution.

the sample silicone membrane is 1 mm. During the process of hydrate formation, the sample silicone membrane is to minimize gas diffusion from the specimen into the cell water. While during the process of shearing test, it is used to prevent membrane puncture under relatively high confining pressures. ③ Seal the vessel and pump water into the confining pressure cavities, which is described as "porous holder" in Fig. 1. Pump methane gas into the cell when confining pressure reached 0.5 MPa. Since outlet of the circulation line located at the bottom of the vessel and inlet located at both side of the vessel. In order to replace the air inside the porous media, we keep inlet closed and outlet open. Methane gas is injected only from the upper inlet. Keep confining pressure larger than pore pressure 0.5 MPa constantly. ④ Turn off outlet, keep both inlet line open, inject methane gas simultaneously from upper and bottom inlet line, increase the confining pressure at the same time. Until pore pressure reaches 4.5 MPa while the confining pressure reaches 5.5 MPa. ⑤ Turn on air bath and set temperature for 1.0°C (±0.5°C) to cool the system and form hydrate for 60 h∼72 h, during which the pore pressure and confining pressure were kept at a constant value, as was descript in step ④. ⑥ According to different experimental demand, effective confining pressure is adjusted for 1 MPa, 2 MPa, 4 MPa, respectively. Set the shear rate for 0.9 mm/min. ⑦ Start shearing test and record shearing data at each 5 s, stress-strain changing behaviors were shown in the coordinate frame timely. In order to forbid hydrate from decomposition, system temperature was kept at 1.0°C (±0.5°C) during shearing test. If no strain-softening phenomena exhibited during the whole shearing procedure, finish shear when axial strain arrives 12%∼15%. Otherwise, finish shear when after-peak stress keeps stable.

2.2 Hydrate saturation determination

Since the capillary effect of marine silica intermediate fine sands can be ignored under constant temperature and constant pressure condition, injected methane and pre-mixed SDS solution can be mixed intensively. All water inside the porous media can be assumed to form hydrate. Then the hydrate saturation in the sediments can be expressed as Eq. (1).

$$S_h = \frac{V_h}{V_\varphi} \times 100\% \tag{1}$$

where, $V_h = \frac{m_h}{\rho_h}$, $m_h = \frac{nM_W + M_c}{nM_W} \cdot m_W$, $m_W = V_W \cdot \rho_W$.

According to the above method, if prime water content in the sediments is 8 mL, 16 mL and 24 mL, the final hydrate saturation in the sediments is about 13.3%, 26.6%, 39.9%, respectively.

2.3 Volumetric strain and lateral strain test method

In the experiments, confining pressure is supplied by tap water, which can be viewed as incompressible liquid under experimental pressure condition. Thus, some of the tap water will be squeezed out while piston is pressed into the cell. The volumetric strain can be expressed as Eq. (2).

$$\varepsilon_v = \frac{\Delta V}{V_0} \times 100\% = \frac{V_{in} - V_{out}}{V_0} \times 100\% \tag{2}$$

Lateral strain along height of the test species is uneven, equivalent lateral strain of the hydrate-bearing sediments can be calculated by the following procedures.

Volume change during shearing process can be expressed as Eq. (3).

$$\Delta V = V_0 - V_1 = \pi(r_0^2 L_0 - r_1^2 L_1) \tag{3}$$

Supposing current lateral strain is ε_l, current axial strain is ε_a. Then Eq. (4) obtained.

$$L_1 = L_0(1 - \varepsilon_a)$$

$$r_1 = r_0(1 - \varepsilon_l) \tag{4}$$

Finally, lateral strain of hydrate-bearing sample under triaxial shearing condition can be derived by combining Eq. (2)∼ Eq. (4).

$$\varepsilon_l = (1 - \sqrt{\frac{1 - \varepsilon_v}{1 - \varepsilon_a}}) \times 100\% \tag{5}$$

3. Shearing behaviors and softening/hardening mechanisms

3.1 Stress-strain properties

As was described above, hydrate saturation in the experimental samples are 0%, 13.3%, 26.6%, 39.9%, respectively. Typical stress-strain curves of unconsolidated hydrate-bearing sediments at different hydrate saturation situations with the same effective confining pressure are depicted from Fig. 3 to Fig. 5. Here we won't focus on the absolute shear strength values of hydrate-bearing samples, but emphasis on the virtual factors that affect failure mode of hydrate-bearing sediments.

Table 1. Failure pattern of unconsolidated hydrate-bearing sands.

	σ_3 = 1 MPa	σ_3 = 2 MPa	σ_3 = 3 MPa
$S_h = 0\%$	Strain-hardening	Strain-hardening	Strain-hardening
$S_h = 13.3\%$	Strain-hardening	Strain-hardening	Strain-hardening
$S_h = 26.6\%$	Strain-softening	Strain-hardening	Strain-hardening
$S_h = 40.0\%$	Strain-softening	Strain-softening	Strain-hardening

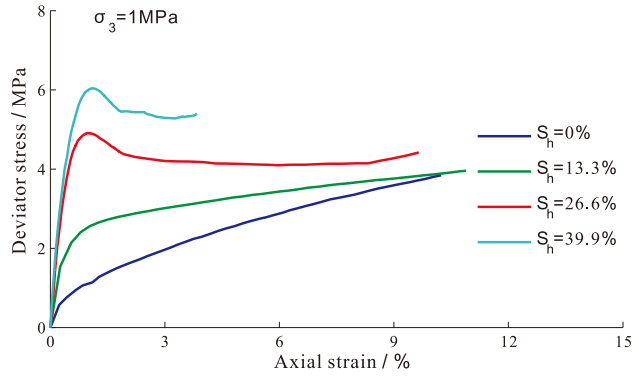

Fig. 3. Typical stress-strain curves while effective confining pressure is 1 MPa.

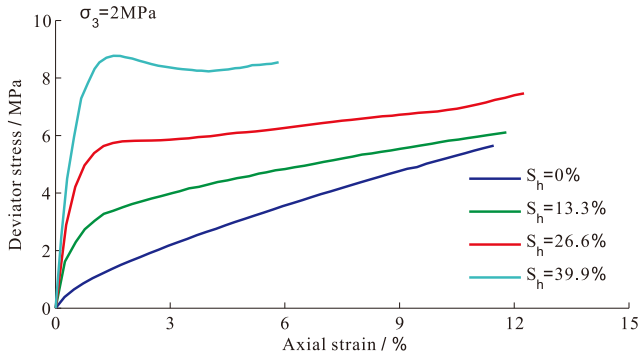

Fig. 4. Typical stress-strain curves while effective confining pressure is 2 MPa.

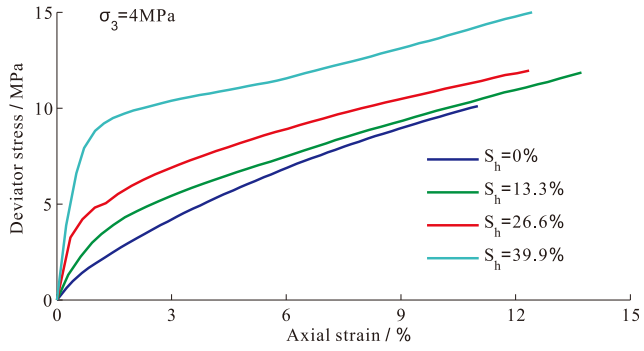

Fig. 5. Typical stress-strain curves while effective confining pressure is 4 MPa.

If the effective confining pressure is 1 MPa, it can be seen from Fig. 3 that for samples with hydrate saturation of 39.9% and 26.6%, failure mode tends to become brittle and their stress-strain curves present to be strain-softening shapes. While for the samples with hydrate saturation of 0% and 13.3%, failure mode tend to become ductile or even plastic, and their stress-strain curves present to be strain-hardening shapes. It's means that for the same species of sediments, with the increase of hydrate saturation, failure mode will change from plastic damage to ductile damage and to the brittle damage mode eventually. The changing behaviors of failure mode can also be proved via Fig. 4 and Fig. 5, where the effective confining pressure is 2 MPa and 4 MPa, respectively. Particularly, all stress-strain curves showed strain-hardening shapes and the failure mode tends to be ductile or plastic when effective confining pressure is 4 MPa (Fig. 5).

On the other hand, we conclude that different effective confining pressure may cause different changing critical values of failure mode. To detect the influence of effective confining pressure on failure mode of hydrate-bearing sediments at the same hydrate saturation situations, we extract stress-strain curves with the same hydrate saturation from Fig. 3 to Fig. 5, and then put them into the same coordinate systems, Fig. 6 ∼Fig. 9 were yielded finally.

Fig. 4 showed unconsolidated sediment's shearing properties without hydrate formation in the porous media. It can be seen that all stress-strain curves showed strain-hardening shapes and the failure mode tend to be plastic damage when without hydrate formation in the porous media. The higher the effective confining pressure, the higher shear strength is, as was known commonly.

It can be infer by comparison of Fig. 6∼Fig. 9 that with the increase of effective confining pressure at the same hydrate saturation condition, the failure mode tends to change from brittle to ductile and will show evident plastic damage if the confining pressure is high enough. By the way, stress-strain curves tend to change from strain-softening to strain-hardening shapes.

The above experimental data showed similar changing trend with the data published by Miyazaki, K., et al. (2011), but different with those published by Shi, Y H., et al. (2015) absolutely, in which the stress-strain curves showed obvious "flat stage" when triaxial strain reach around 6%. This may be caused by the difference between the particle size and continent of the sediment itself.

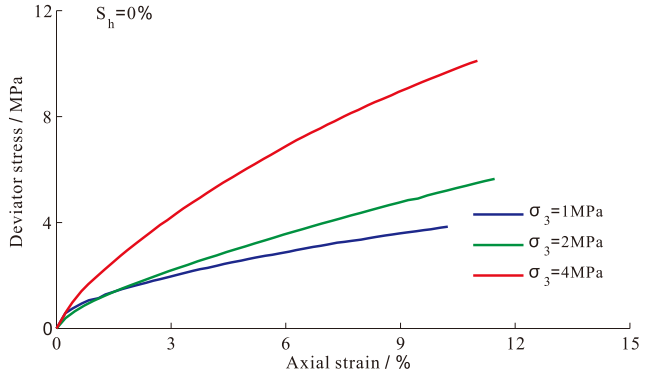

Fig. 6. Effective confining pressures influence on stress-strain curves when S_h = 0% .

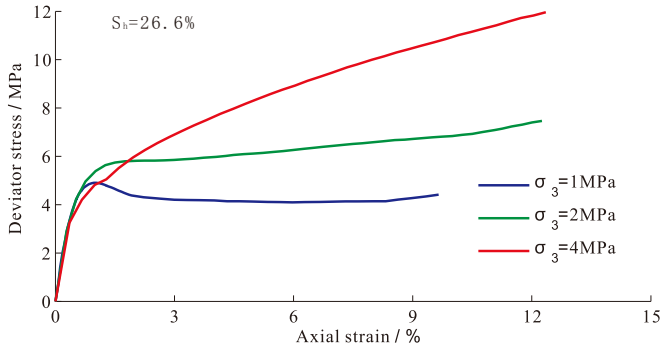

Fig. 8. Effective confining pressures influence on stress-strain curves when S_h = 26.6%.

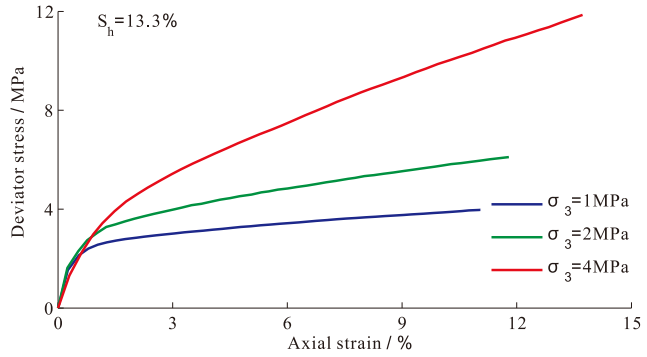

Fig. 7. Effective confining pressures influence on stress-strain curves when S_h = 13.3%.

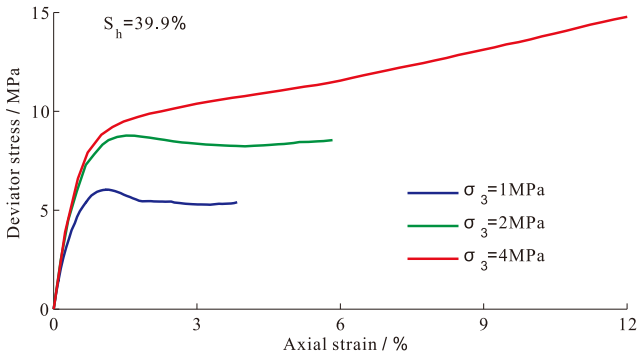

Fig. 9. Effective confining pressures influence on stress-strain curves when S_h = 39.9%.

3.2 Softening/Hardening mechanisms

As was discussed above, 12 groups of typical triaxial shearing experiments were done and their homologous failure pattern was summarized in Table 1.

According to critical state theory of Sandy soil, in the critical void ratio versus average effective stress coordinate system, Top right of the critical state line is characterized as “soften plane”, while bottom left of the critical state line is characterized as “harden plane”, as was shown in Fig. 10.

During the process of triaxial shearing test, all samples’ state will tend to progress toward the critical state line, wherever the original state located or however its stress state changes. Therefore, samples with an original state located at soften plane will tend to come close to the critical state line and may lead obvious dilatancy effect, and the dilatancy effect will be shown as strain-softening properties of the stress-strain curves. In another way, samples with an original state located at harden plane will tend to come close to the critical state line and may lead obvious shrinkage effect, and the shrinkage effect will be shown as strain-hardening properties of the stress-strain curves.

As for hydrate-bearing sediments, hydrate can be viewed as part of the skeleton. Therefore, formation of gas hydrate will decrease the void ratio of the sediment. For the same kind of sediment, same hydrate saturation may lead same void ratio of the hydrate-bearing sediments. If the confining pressure is small enough, the original state of the sample may locate at point A in Fig. 10. Since samples located at A belongs to harden plane, sample’s stress state should tend to come close to the critical state line and may lead obvious shrinkage effect, and the shrinkage effect will be shown as strain-hardening properties of the stress-strain curves. In addition, if the confining pressure is high enough, the original state of the sample may locate at point C in Fig. 10. Since samples located at C belongs to soften plane, samples stress state should tend to come close to the critical state line and may lead obvious dilatancy effect, and the dilatancy effect will be shown as strain-softening properties of the stress-strain curves, which was already described above.

Since hydrate can be viewed as part of the skeleton, the higher the hydrate saturation, the lower the void ratio. If the hydrate saturation is high enough, the void ratio may be low and the original state of the sample may locate at point D in Fig. 10. Since samples located at D belongs to harden plane, sample’s stress state should tend to come close to the critical state line and may lead obvious shrinkage effect, and the shrinkage effect will be shown as strain-hardening properties of the stress-strain curves. On the contrary, if the hydrate saturation is low enough, the void ratio may be high and the

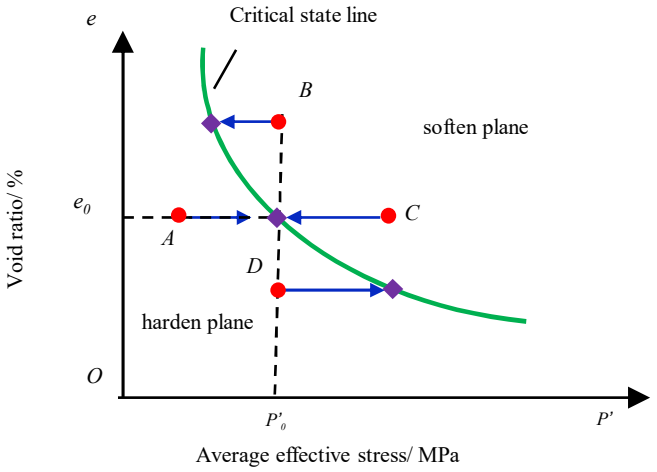

Fig. 10. Stress path of unconsolidated hydrate-bearing sands in $e-p'$ plane.

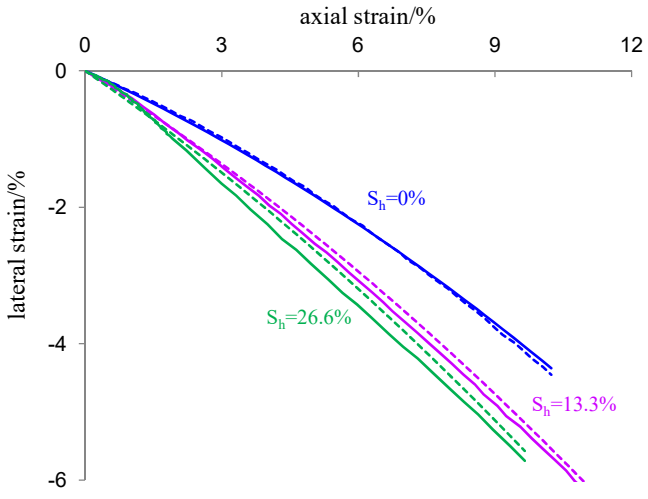

Fig. 11. Experimental (solid lines) and calculated (broken lines) axial-lateral strain relationships when effective confining pressure is 1 MPa.

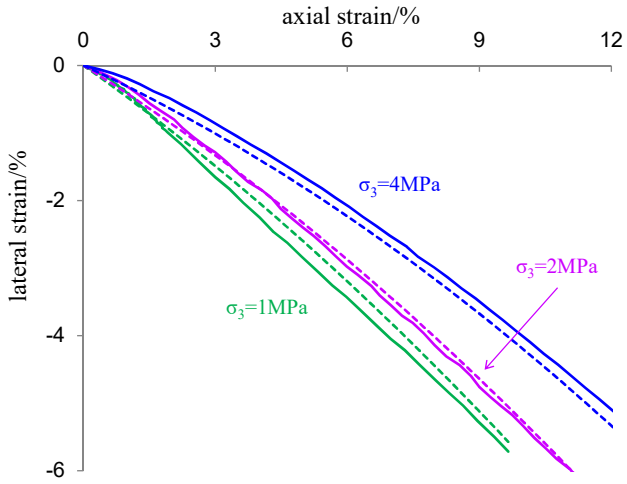

Fig. 12. Experimental (solid lines) and calculated (broken lines) axial-lateral strain relationships when hydrate saturation is 26.6%.

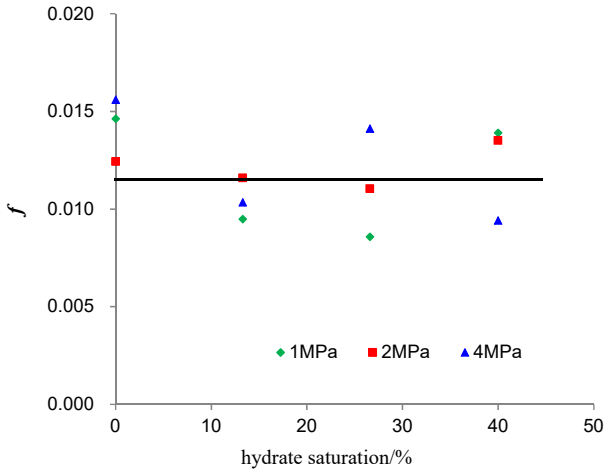

Fig. 13. f variation with hydrate saturation and confining pressure.

original state of the sample may locate at point B in Fig. 10. Since samples located at B belongs to soften plane, sample's stress state should tend to come close to the critical state line and may lead obvious dilatancy effect, and the dilatancy effect will be shown as strain-hardening properties of the stress-strain curves, which was already described above.

All in all, critical state theory is the root cause of failure pattern of hydrate-bearing sediments.

4. Axial-lateral strain relationship models

4.1 Axial-lateral strain relationship modeling process

Generally, axial stress-strain curves can be matched by different kind of constitutive models (Li et al., 2016). However, these constitutive models didn't contain effective factors that can describe axial-lateral strain relationships for hydrate-bearing sediments.

Lateral strain was calculated via Eq. (5) in this study. A basic semi-empirical model for axial-lateral strain relationships has been provided by Miyazaki, et al. (2012).

$$\varepsilon_1 = -f\varepsilon_a^2 - g\varepsilon_a \qquad (f>0, g>0) \tag{6}$$

Typical axial-lateral strain curves of unconsolidated hydrate-bearing sediments at different hydrate saturation situations and different effective confining pressure were shown in Fig. 11 and Fig. 12, respectively, where solid lines represent experimental result while broken lines represent calculated result by Eq. (6).

For further study, all experimental data were fitted by Eq. (6) and corresponding model coefficients were shown in Fig. 13 and Fig. 14, respectively.

It can be seen from Fig. 13 that f values for different experimental conditions lie in the range defined by 0.009 and 0.015. For simplicity, average of all f values (f = 0.012) was

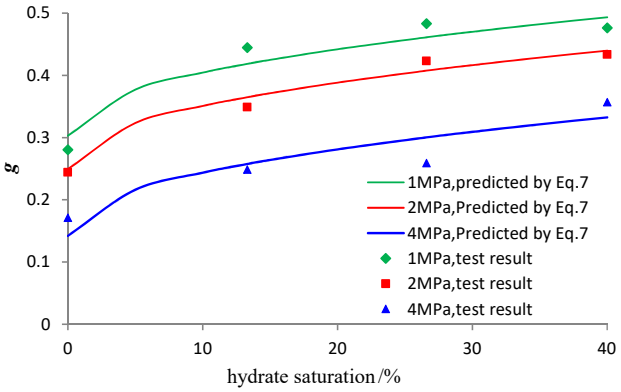

Fig. 14. g variation with hydrate saturation and confining pressure.

taken as the final model coefficient for unconsolidated hydrate-bearing sediments.

On the other hand, g values increase with the increase of hydrate saturation, but decrease with the increase of effective confining pressure. An empirical model can be obtained by least-square regression for the data showed in Fig. 14.

$$g = a_2 S_h^{n_2} + b_2 \sigma_3 + c_2 \tag{7}$$

where, n_2, a_2, b_2 and c_2 are factors, a_2 = -0.2887, b_2 = -0.0536, c_2 = 0.3566 and n_2 = 0.4543.

4.2 Physical meaning of model coefficients

It can be easily concluded from Eq. (6) that absolute value of the slope for axial-lateral lines is tangent Passion's ratio. Which can be written as Eq. (8).

$$\mu_t = -\frac{\mathrm{d}\varepsilon_l}{\mathrm{d}\varepsilon_a} = 2f \cdot \varepsilon_a + g \tag{8}$$

Then, Initial tangent Passion's ratio can be obtained if we take ε_a = 0 in Eq. (8).

$$\mu_i = -\frac{\mathrm{d}\varepsilon_l}{\mathrm{d}\varepsilon_a}|_{\varepsilon_a=0} = g \tag{9}$$

The above equation indicates that g values in Fig. 14 just reflect changing rules of initial tangent Passion's ratio under different experimental condition. Initial tangent Passion's ratio decrease with the increase of confining pressure and the decrease of hydrate saturation. Furthermore, different model coefficients' effect on strain relationships are different, probing into the physical meaning of each coefficient is essential for further understanding of strain relationships.

5. Strength and modulus parameters evolution rules

5.1 Tangent modulus

Tangent modulus is the slope of the tangent line of stress-strain curves. Tangent modulus can be used to describe real-time deformation modulus during the whole process of triaxial shearing procedure. Fig. 15 shows typical tangent modulus of unconsolidated hydrate-bearing sands under different hydrate saturation and different effective confining pressure. As was supposed previously, tangent modulus is of strong correlation with failure pattern. Under strain-hardening failure pattern, value of tangent modulus decreases rapidly with the increase of axial train, and then keeps relatively constant. What's more, tangent modulus keeps positive in all axial train variation range. Nevertheless, under strain-softening failure pattern, with the increase of axial strain, tangent modulus decreases from a very high positive value until negative "peak point", and then keeps relatively constant around zero by a slight uplift. The marginal value of tangent modulus from positive value to negative value represents peak strain of hydrate-bearing sediments.

Wei, H.Z., et al. (2011) has indicated the feasibility of Eq. (10) in description of tangent modulus hydrate-bearing sediments.

$$E_{tan} = E_0(1 + \frac{\varepsilon_a}{\tau_{max}/E_0})^{-2} \tag{10}$$

However, after direct comparison between form of Eq. (10) and Fig. 13, we found that Eq. (10) is not descriptive enough to completely describe tangent modulus when axial strain exceeds peak strain, where tangent modulus become negative. It means that Eq. (10) is suitable only for strain-hardening failed hydrate-bearing sediments. An immaculate tangent modulus prediction model should be discussed within each failure pattern, and further research should be done in order to establish a quantized tangent modulus prediction model for unconsolidated hydrate-bearing sediments.

5.2 Peak strength and Peak modulus

Peak strength represents ultimate deviator stress strength in triaxial shearing experiments. As for strain-softening failed hydrate-bearing samples, peak value of axial stress can be taken as peak strength directly. Otherwise, axial stress when axial strain arrives 12% was taken as the peak strength of hydrate-bearing samples in this paper. Fig. 16 explicates basic changing rules of peak strength with the change of effective confining pressure and hydrate saturation. It can be seen from Fig. 16 that peak strength increases almost linearly with effective confining pressure, despite of strain-hardening failure pattern or strain-softening failure pattern. Similarly, although nonlinear variation rules showed, peak strength increase with hydrate saturation independent of failure pattern.

Specific value of peak strength and corresponding axial strain represents deformation modulus when hydrate-bearing sediments was destructed under triaxial stress. Deformation modulus at peak strength point can be defined as peak modulus. Typical peak modulus evolution curves of unconsolidated hydrate-bearing sedimentss with hydrate saturation and effective confining pressure were shown in Fig. 17.

Fig. 17 showed very interesting phenomena because the results in Fig. 17 are of great correspondence with the failure pattern summarized in Table 1. Under strain-hardening failure

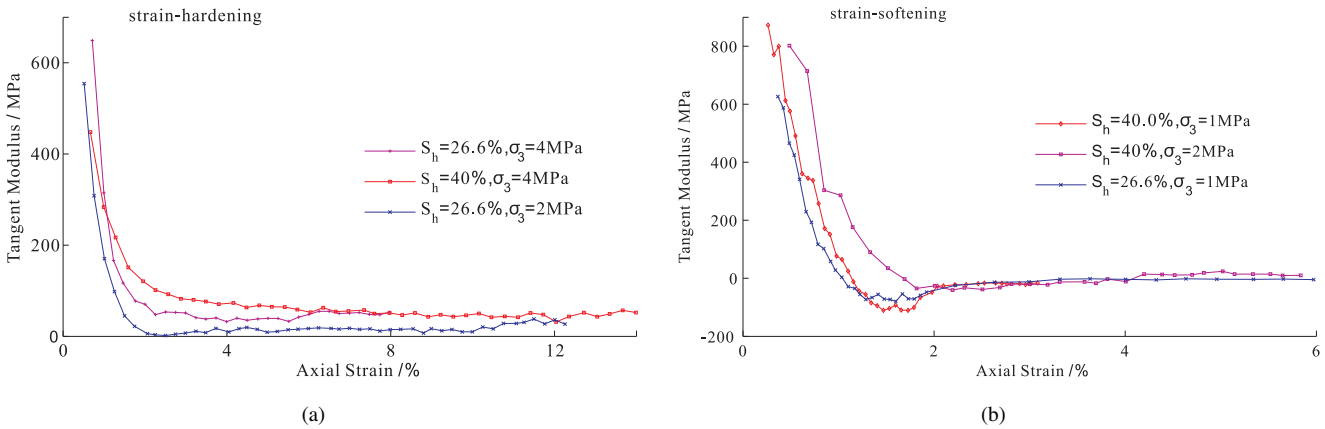

Fig. 15. Changing rules of tangent modulus with axial strain.

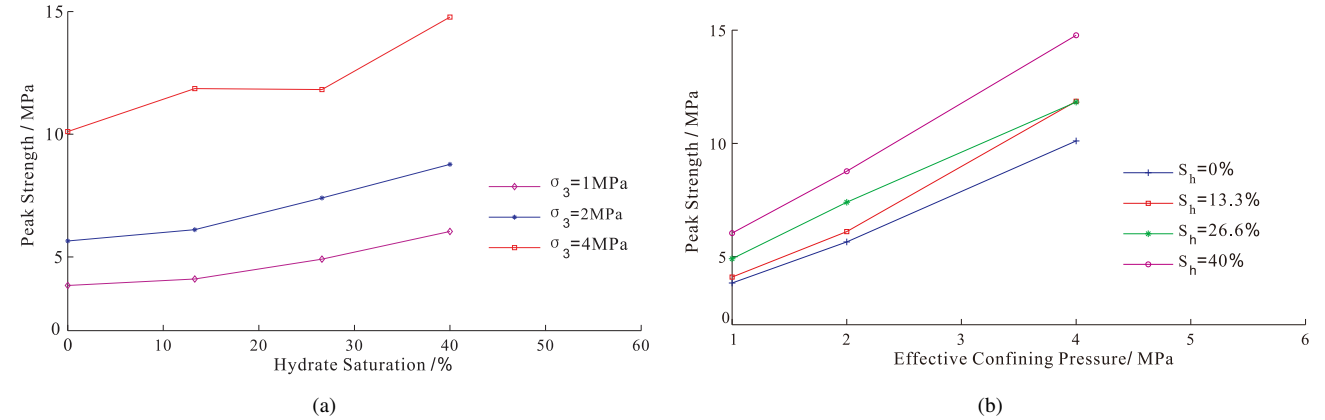

Fig. 16. Peak strength evolution rules for unconsolidated hydrate-bearing sediments.

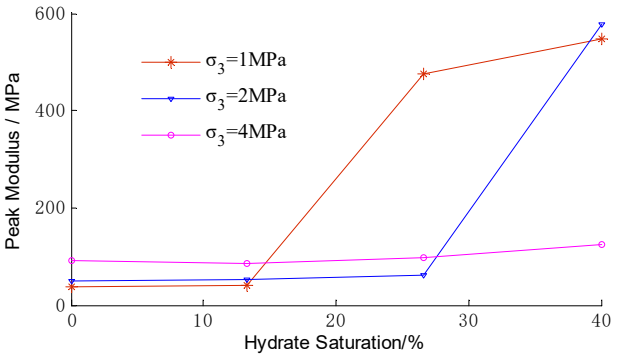

Fig. 17. Peak modulus of unconsolidated hydrate-bearing sands.

pattern condition, peak strength increases slightly with the increase of hydrate saturation and effective confining pressure. However, there was a value zoom for peak strength with the changing of combination of hydrate saturation and effective confining pressure, which indicates changes of failure pattern from strain-hardening to strain-softening.

The above conclusions are very important for hydrate exploitation test operation because of the following reason. As was described above, high-hydrate-saturated formations are of strain-softening failure pattern normally. With the progress of producing natural gas from hydrate-bearing reservoir, hydrate saturation decreased. It means that sudden change of failure pattern maybe happen during the process of hydrate exploitation, which indicates sudden decrease of formation modulus. Hydrate exploitation test operation may be forced to face some probabilistic risks because of sudden decrease of formation modulus. Therefore, compressive study on critical condition of failure pattern is of vital importance for hydrate exploitation in specialized hydrate-bearing reservoirs.

6. Conclusion and outlook

1. Failure mode of hydrate-bearing sediments is controlled by several parameters, such as effective confining pressure, hydrate saturation, etc. The principle of critical state controlled mechanism of strain softening and/or hardening failure mode basically for hydrate-bearing intermediate fine sediments.

2. Initial tangent Passion's ratio decrease with the increase of confining pressure and the decrease of hydrate saturation. Furthermore, different model coefficients' effect on strain relationships are different, probing into the physical meaning of each coefficient is essential for further understanding of strain relationships.

3. Models proposed here maybe only suitable for descrip-

tion of hydrate-bearing intermediate fine sediments, In order to detect strength properties of other hydrate-bearing sediments, further laboratory study is needed.

4. With the progress of producing natural gas from hydrate-bearing reservoir, sudden change of failure pattern and sudden decrease of formation modulus maybe happen. To avoid engineering operation risks, compressive study on critical condition of failure pattern is needed for hydrate exploitation in specialized hydrate-bearing reservoirs.

Nomenclature

m_w = mass of SDS solution, g

m_h = mass of hydrate, g

ρ_w = density of SDS solution, g/cm^3

ρ_h = density of hydrate, g/cm^3

V_w = volume of SDS solution, g/cm^3

V_h = volume of hydrate, g/cm^3

V_ϕ = pore volume of sediment in the silicone membrane, g/cm^3; V_ϕ =77.9 g/cm^3

V_{in} ,V_{out} = the volume of piston pressed into the cell and the volume of tap water squeezed out of the cell, g/cm^3

V_0 = the prime volume of the test species, g/cm^3

r_0, r_1 = prime radius and current radius of the test species during shearing test, cm

L_0, L_1 = prime height (120 mm) and current height of the test species during shearing test, cm

E_0 = initial tangent modulus, MPa

τ_{max} = shearing strength, MPa

ε_a = axial strain, %

f, g = model coefficients that can be decided via least-squares approximation method for different experimental data

Acknowledgments

This research was supported by National Natural Science Foundation of China (41606078); National Key Research and Development Plan (2017YFC0307600); and Qingdao National Laboratory for Marine Science and Technology (QNLM2016ORP0203, QNLM2016ORP0207).

References

Hyodo, M., Nakata, Y., Yoshimoto, N., et al. Shear behavior of methane hydrate-bearing sand. Paper ISOPE-I-07-428 Presented at the Proceedings of the Seventeenth International Offshore and Polar Engineering Conference, Lisbon, Portugal, 1-6 July, 2007.

Hyodo, M., Li, Y., Yoneda, J., et al. Effects of dissociation on the shear strength behavior of methane hydrate-bearing sediments. Mar. Petrol. Geol. 2013, 51(2): 52-62.

Li, L.D., Cheng, Y.F., Sun, X.J., et al. Experimental sample preparation and mechanical properties study of hydrate-bearing sediments. J. China Univ. Pet. Ed. Nat. Sci. 2012, 36(4): 97-101.

Li, Y.H., Song, Y.C., Liu, W.G., et al. Temperature and shear rate influences on hydrate-bearing soils. Natural Gas Exploration and Development 2012, 35(1): 50-53.

Li, Y.H., Song, Y.C., Yu, F., et al. Effect of confining pressure on mechanical behavior of methane hydrate-bearing sediments. Petrol. Explor. Develop. 2011, 38(5): 637-640.

Li, Y.L., Liu, C.L., Liu, L.L., et al. The mechanical properties of methane hydrate-bearing unconsolidated sediment. J. China Univ. Pet. Ed. Nat. Sci. 2017, 41(3): 1-9.

Li, Y.L., Liu, C.L., Liu, L.L., et al. Triaxial shear test and strain analysis of unconsolidated hydrate-bearing sediments. Nat. Gas Geosci. 2017, 28(3): 383-390.

Li, Y.L., Liu, C.L., Liu, L.L., et al. Key Issues for Triaxial Test of Hydrate-Bearing Sediment (In Chinese). Advance in New and Renewable Energy 2016, 4(4): 279-285.

Li, Y.L., Liu, C.L., Liu, L.L. Damage statistic constitutive model of hydrate-bearing sediments and the determination method of parameters (In Chinese). Acta Petrol. Sin. 2016, 37(10): 1273-1279.

Liu, F., Kou, X.Y., Jiang, M.J., et al. Triaxial shear strength of synthetic hydrate-bearing sediments. Chin. J. Geotech. Eng. 2013, 35(8): 1565-1572.

Liu, W.T., Shi, Y.H., Zhang, X.H., et al. Geo-technical features of the seabed soils in the east of Xisha trough and the mechanical properties of gas hydrate-bearing fine deposits. Mar. Geol. Quat. Geol. 2014, 34(3): 39-47.

Liu W., Chen Y., Zhu, Y., et al. Effects of different mining methods on the strength behavior of gas hydrate-bearing sediments. Energy Procedia 2014, 61: 547-551.

Lu, X.B., Wang, L., Wang, S.Y., et al. Triaxial test on THF hydrate-bearing sediment. Presented at 13th China national ocean science symposium, Nanjing, Jiangsu Province, China, 19-20 September, 2007.

Masui, A., Haneda, H., Ogata, Y., et al. Mechanical properties of sandy sediment containing marine gas hydrates in deep sea offshore Japan. Paper ISOPE-M-07-015 Presented at the Proceedings of the International Society of Offshore and Polar Engineers Ocean Mining Symposium, Lisbon, Portugal, 1-6 July, 2007.

Miyazaki, K., Masui, A., Sakamoto, Y., et al. Triaxial compressive properties of artificial methane-hydrate-bearing sediment. J. Geophys. Res. 2011,116(B6): B06102.

Miyazaki, K., Tenma, N., Aoki, K., et al. A nonlinear elastic model for triaxial compressive properties of artificial methane-hydrate-bearing sediment samples. Energies 2012, 5(10): 4057-4075.

Priest, J.A., Clayton, C.R.I., Rees, E.V.L. Potential impact of gas hydrate and its dissociation on the strength of host sediment in the Krishna-Godavari Basin. Mar. Petrol. Geol. 2014, 58: 187-198.

Shi, Y.H., Zhang, X.H., Lu, X.B., et al. Experimental study on the static mechanical properties of hydrate-bearing silty-clay in China South Sea. Chin. J. Theor. Appl. Mech. 2015, 47(3): 521-528.

Sun, X.J., Cheng, Y.F., Li, L.D., et al. Triaxial compression test on synthetic core sample with simulated hydrate-bearing sediments. Pet. Drill. Tech. 2012, 40(4): 52-57.

Wei, H.Z., Yan, R.T., Chen, P., et al. Deformation and failure

behavior of carbon dioxide hydrate-bearing sands with different hydrate contents under triaxial shear tests. Rock Soil Mech. 2011, (S2): 198-203.

Winters, W.J., Waite, W.F., Mason, D.H., et al. Methane gas hydrate effect on sediment acoustic and strength properties. J. Pet. Sci. Eng. 2007, 56(s1-3): 127-135.

Winters, W.J., Wilcox, C.R.W., Long, P., et al. Comparison of the physical and geotechnical properties of gas-hydrate-bearing sediments from offshore India and other gas-hydrate-reservoir systems. Mar. Pet. Geol. 2014, 58: 139-167.

Wu, N.Y., Huang, L., Hu, G.W., et al. Geological controlling factors and scientific challenges for offshore gas hydrate exploration. Mar. Geol. Quat. Geol. 2017, 37(5): 1-11.

Yan, R.T., Wei, C.F., Wei, H.Z., et al. Effect of hydrate formation on mechanical strength of hydrate-bearing sand. Chin. J. Geotech. Eng. 2012, (7): 1234-1240.

Yan, R.T., Wei, H.Z., Fu, X.H., et al. Influence of occurrence mode of hydrate on mechanical behavior of hydrate-bearing soils. Chin. J. Rock Mech. Eng. 2013, (S2): 4115-4122.

Yoneda, J., Masui, A., Konno, Y., et al. Mechanical behavior of hydrate-bearing pressure core sediments visualized under triaxial compression. Mar. Pet. Geol. 2015, 66: 451-459.

Yu, F., Song, Y.C., Li, Y.H., et al. A study on stress-strain relations of methane hydrates. Acta. Petrol. Sin. 2011, 32(4): 687-692.

Yun, T.S., Santamarina, J.C., Ruppel, C. Mechanical properties of sand, silt, and clay containing tetrahydrofuran hydrate. J. Geophys. Res. Atmos. 2007, 112(B4): 93-101.

Zhang, X.H., Wang, S.Y., Li, Q.P., et al. Experimental study of mechanical properties of gas hydrate deposits. Rock Soil Mech. 2010, 31(10): 3069-3074.

Zhang, X.H., Lu, X.B., Wang, S.Y., et al. Experimental study of static and dynamic properties of tetrahydrofuran hydrate-bearing sediments. Rock Soil Mech. 2011, 32(S1): 303-308.

Zhang, H.T., Zhang, H.Q., Zhu, Y.H. Gas hydrate investigation and research in China: Present status and progress. Geol. China 2007, 34(6): 953-961.